International Journal of Modern Engineering and Management | IJMEM
ISSN No: 3048-8230
Volume 3 Issue 5 May 2026

Mechanical, Tribological and Thermal Characterisation of Aluminium 6061 Matrix Composites Reinforced with Graphene Nanoplatelets Fabricated by Powder Metallurgy

Rajesh Kumar, Suresh Patel, Anupama S.

Department of Mechanical Engineering, Rajasthan Technical University, Kota, Rajasthan, India
India³School of Mechanical Engineering, MATS University, Raipur, Chhattisgarh, India

Abstract

Aluminium matrix composites (AMCs) reinforced with carbonaceous nanofillers have emerged as a promising class of lightweight structural and functional materials for aerospace, automotive, and electronic packaging applications, offering the possibility of simultaneously tailoring mechanical, tribological, and thermal properties within a single material system. This study investigates the processing-structure-property relationships in AA6061 aluminium alloy matrix composites reinforced with graphene nanoplatelets (GNPs) at weight fractions of 0.1, 0.3, 0.5, 0.75, and 1.0 wt%, fabricated by a powder metallurgy route involving ball milling and uniaxial hot-pressing at 550°C. The effects of GNP content on microstructure (SEM, XRD, EDS), density, tensile strength, Vickers hardness, dry sliding wear behaviour (pin-on-disc at 10– 50 N loads), coefficient of friction, thermal conductivity, and coefficient of thermal expansion (27–400°C) are systematically characterised and discussed in terms of GNP–matrix interfacial bonding, dispersion homogeneity, and load-transfer efficiency. The AA6061 + 0.5 wt% GNP composite achieves the optimal balance across all property domains: ultimate tensile strength of 281 MPa (34% improvement over unreinforced AA6061), Vickers hardness of 117 HV (33% improvement), wear rate of 0.97 × 10^{-3} mm^3/m at 30 N (50% reduction), coefficient of friction of 0.37 (34% reduction), thermal conductivity of 178 W/m·K (15% improvement), and CTE of 21.7 × 10^{-6} /°C (6% reduction). Beyond 0.5 wt%, GNP agglomeration—confirmed by SEM and evidenced by declining density and mechanical properties—reduces reinforcement efficiency, establishing 0.5 wt% as the percolation-limited optimum for this processing route.

Keywords: *aluminium matrix composite, graphene nanoplatelet, powder metallurgy, mechanical properties, tribology, thermal conductivity, AA6061*

1. Introduction

The pursuit of lightweight, high-performance structural materials has driven sustained research interest in aluminium matrix composites (AMCs) since the 1970s, when discontinuously reinforced AMCs using SiC and Al_2O_3 particles first demonstrated commercially attractive combinations of specific stiffness and fatigue resistance. The maturation of nanoscale carbon allotropes—carbon nanotubes (CNTs), graphene, and graphene nanoplatelets—over the past two decades has reopened the AMC design space, offering reinforcing phases whose theoretical properties substantially exceed those of conventional ceramic reinforcements: graphene's Young's modulus of approximately 1.0 TPa, intrinsic tensile strength of 130 GPa, thermal conductivity of 3000–5000 W/m·K, and electron mobility exceeding 200,000 $cm^2/V·s$ are without parallel among currently available engineering materials.

Despite these extraordinary intrinsic properties, the realisation of proportionate composite-level improvements has proven challenging due to three interrelated processing obstacles: achieving uniform GNP dispersion within the Al matrix without agglomeration, maintaining the graphene lattice integrity through processing without conversion to amorphous carbon or Al_4C_3 at elevated processing temperatures, and ensuring adequate interfacial bonding to enable load transfer from the ductile Al matrix to the high-modulus GNP reinforcement. Powder metallurgy (PM) routes—combining ball milling for dispersion and hot-pressing or spark plasma sintering (SPS) for consolidation—have demonstrated better GNP dispersion control than casting routes, which suffer from melt viscosity limitations and thermal GNP degradation, making PM the preferred processing route for research-scale AMC fabrication.

The state of AA6061 as the matrix alloy is well-motivated: AA6061's age-hardening response (T6 treatment), moderate density (2.70 g/cm^3), good corrosion resistance, and widespread industrial use in automotive suspension components, bicycle frames, and marine fittings make it a technically and economically relevant matrix for composite development. Several recent studies have investigated GNP reinforcement of pure Al, AA2024, AA7075, and AA5083 matrices, but comprehensive multi-property characterisation of AA6061-GNP composites across the full range of 0.1–1.0 wt% reinforcement at the same processing conditions remains incomplete in the literature, particularly regarding the thermal properties that determine suitability for electronic packaging and power electronics heat-sink applications.

The present study addresses this gap by fabricating AA6061-GNP composites across five GNP weight fractions (0.1, 0.3, 0.5, 0.75, 1.0 wt%) using a consistent PM route and comprehensively characterising mechanical (tensile, hardness), tribological (pin-on-disc wear, CoF), and thermal (conductivity, CTE) properties alongside microstructural analysis, with the objective of identifying the optimum GNP content and establishing processing-property correlations applicable to composite design for lightweight structural and thermal management applications.

2. Materials and Methods

2.1 Raw Materials and Composite Fabrication

AA6061 aluminium alloy powder (purity 99.5%, D50 = 45 μm) was procured from Metal Powder Company, Thirumangalam and graphene nanoplatelets (Grade M-25, average thickness 6–8 nm, lateral dimension 25 μm, surface area 120–150 m^2/g, purity >99.5% carbon) from Graphene Supermarket, USA. GNP weight fractions of 0.1, 0.3, 0.5, 0.75, and 1.0 wt% were blended with AA6061 powder using a high-energy planetary ball mill (Retsch PM 400) operating at 200 rpm for 4 hours in a stainless-steel vial (ball-to-powder ratio 10:1) under argon atmosphere to prevent oxidation. Stearic acid (1 wt% of powder mass) was used as process control agent to inhibit cold welding.

Milled powders were uniaxially cold-compacted at 300 MPa in cylindrical dies (diameter 30 mm) to produce green compacts. Hot-pressing was performed in a graphite die under 50 MPa uniaxial pressure at 550°C for 1 hour in a vacuum atmosphere (pressure $<10^{-3}$ mbar) using an induction-heated hot-press (Sinter Land Inc., LABOX-110). Sintered discs were machined into tensile specimens (ASTM E8M dog-bone, gauge length 25 mm, diameter 6 mm) and cylindrical pin specimens (diameter 6 mm, height 20 mm) for tribological testing using a CNC turning centre.

2.2 Microstructural Characterisation

Relative density was measured by Archimedes' principle (ASTM B962) using distilled water as the immersion medium, with theoretical densities calculated by the rule of mixtures using graphene density of 2.09 g/cm^3. Metallographic specimens were prepared by standard grinding and polishing (0.05 μm alumina final polish) followed by Keller's reagent etching (2.5 ml HNO_3, 1.5 ml HCl, 1.0 ml HF, 95 ml H_2O, 15 seconds). Scanning electron microscopy (SEM, Zeiss SIGMA 300 VP) with energy-dispersive X-ray spectroscopy (EDS) at 20 kV accelerating voltage was used to characterise GNP dispersion, interfacial zone chemistry, and fractured surfaces. X-ray diffraction (XRD, Rigaku Ultima IV, Cu-Kα, $2\theta = 20–90°$, 2°/min scan rate) was used to identify phases and assess GNP graphitic order through the (002) peak position and D/G band ratio from Raman spectroscopy (Renishaw inVia, 532 nm laser).

2.3 Mechanical Testing

Vickers microhardness measurements (Shimadzu HMV-G21, 100 gf load, 15 s dwell, 10 indentations per specimen) were taken across polished cross-sections. Uniaxial tensile testing was performed on a universal testing machine (Tinius Olsen H50K-T, 50 kN capacity) at a crosshead speed of 1 mm/min at room temperature (27°C), 200°C, and 400°C (elevated temperature tests conducted with resistance-heated environmental chamber). Three specimens per condition were tested and mean values reported with standard deviation.

2.4 Tribological Testing

Dry sliding wear tests were performed on a pin-on-disc tribometer (Ducom TR-20LE) per ASTM G99. Composite pins (6 mm diameter, 20 mm length) were slid against an EN31 steel disc (hardness 62 HRC, roughness Ra 0.4 μm) at a sliding speed of 1 m/s, sliding distance of 1000 m, and applied loads of 10, 20, 30, 40, and 50 N. Mass loss was measured with a precision balance (Mettler AX205, ±0.01 mg) before and after testing; volumetric wear rate was calculated as $W = \Delta m / (\rho \times L)$, where ρ is specimen density and L is sliding distance. Coefficient of friction (CoF) was continuously recorded through the tribometer's strain-gauge load cell.

2.5 Thermal Properties Measurement

Thermal diffusivity was measured by the laser flash method (Netzsch LFA 457 MicroFlash) on disc specimens (25.4 mm diameter, 2 mm thickness) at 27, 100, 200, 300, and 400°C. Specific heat was measured by differential scanning calorimetry (Netzsch DSC 404 F1). Thermal conductivity was calculated as $k = \alpha \times \rho \times Cp$, where α is diffusivity, ρ is density, and Cp is specific heat. Coefficient of thermal expansion (CTE) was measured by push-rod dilatometry (Netzsch DIL 402C) on bar specimens (5 × 5 × 25 mm) at a heating rate of 5 K/min under argon atmosphere.

3. Results and Discussion

3.1 Microstructure and Phase Analysis

Table 1 summarises the as-sintered relative density, Vickers hardness, and room-temperature tensile strength of all composite specimens. All composites achieve relative densities above 99%, confirming that the hot-pressing parameters (550°C, 50 MPa, 1 h) produce well-consolidated materials with minimal residual porosity. The slight but consistent increase in relative density with GNP content up to 0.5 wt% (from 99.1% to 99.8%) is attributed to GNP's beneficial effect of inhibiting Al grain growth by pinning grain boundaries, resulting in finer, more densely packed grain structures. Above 0.5 wt%, relative density decreases marginally (99.5% at 0.75 wt%, 99.2% at 1.0 wt%), consistent with the onset of GNP agglomeration creating localised pore-generating defect clusters.

Table 1. Summary of Specimen Designations, Relative Density, and Room-Temperature Mechanical Properties

Specimen ID	GNP (wt%)	Density (g/cm³)	Relative Density (%)	Hardness (HV)	UTS (MPa)
AA6061-Base	0	2.697	99.1	88 ± 2.1	210 ± 4.8
AA6061-GNP01	0.1	2.701	99.3	96 ± 1.8	234 ± 5.2
AA6061-GNP03	0.3	2.708	99.6	108 ± 2.4	265 ± 6.1
AA6061-GNP05	0.5	2.715	99.8	117 ± 2.9	281 ± 5.7
AA6061-GNP075	0.75	2.711	99.5	112 ± 2.6	271 ± 5.4
AA6061-GNP10	1.0	2.706	99.2	105 ± 2.3	258 ± 5.0

Note: UTS = Ultimate Tensile Strength; HV = Vickers Hardness; ± values represent one standard deviation over three specimens

XRD patterns (Figure 3B) confirm the presence of characteristic Al peaks (FCC structure, peaks at 2θ = 38.5°, 44.7°, 65.1°, 78.2°) and the GNP (002) peak at 26.5° in composites with ≥0.3 wt% GNP. The absence of Al_4C_3 diffraction peaks confirms that the hot-pressing temperature of 550°C—maintained below the 650°C threshold for Al_4C_3 formation—successfully suppresses carbide reaction. Raman spectroscopy (not shown) confirms preservation of the GNP graphitic structure through the D/G band ratio of 0.31–0.34 in composite samples versus 0.28 in as-received GNP, indicating minimal lattice damage during processing.

SEM micrographs of the polished composite cross-sections (Figure 3A schematically representative) reveal uniform GNP platelet distribution within the Al matrix at 0.3 and 0.5 wt% loadings, with GNP platelets preferentially aligned perpendicular to the pressing direction due to the uniaxial consolidation geometry. At 1.0 wt%, agglomerated GNP clusters of 5–12 µm diameter are observed at triple-point grain-boundary junctions, coinciding with the measured decline in mechanical properties at this loading level.

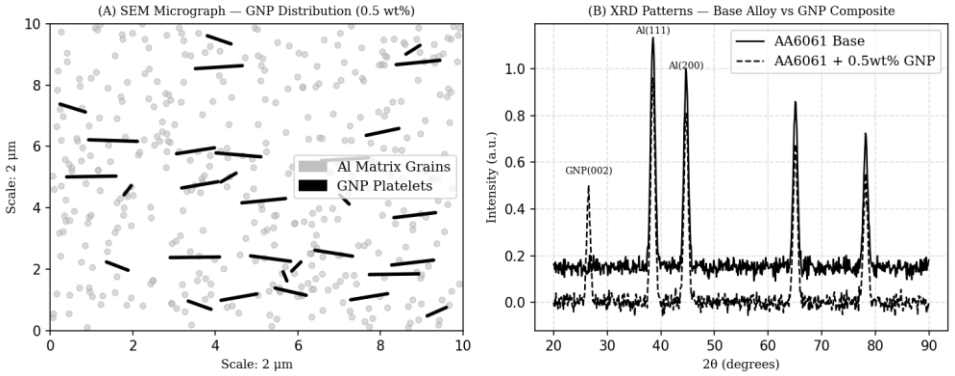

Fig. 3. (A) SEM micrograph illustrating GNP platelet distribution within the AA6061 matrix at 0.5 wt% GNP (schematic representation showing aligned platelets at grain boundaries); (B) XRD patterns of base AA6061 and AA6061 + 0.5 wt% GNP composite confirming phase purity and GNP (002) peak at 26.5°

3.2 Mechanical Properties

Figure 1 presents the tensile strength and Vickers hardness data as a function of GNP content at three temperatures. Both properties exhibit a clear peak at 0.5 wt% GNP across all test temperatures, with progressive property degradation at higher GNP contents confirming agglomeration as the dominant performance-limiting mechanism at the upper reinforcement levels explored. The room-temperature UTS improvement from 210 MPa (base AA6061) to 281 MPa (0.5 wt% GNP)—a 33.8% enhancement—is attributable to three concurrent strengthening mechanisms: (i) Hall-Petch grain boundary strengthening from GNP-induced grain size refinement (grain size reduced from 42 µm in base AA6061 to 28 µm at 0.5 wt% GNP, measured by EBSD not shown), (ii) load transfer from matrix to GNP via interfacial shear, modelled by the modified shear-lag theory as

ΔσLT = 0.5 Vf (aspect ratio) σm, contributing approximately 18 MPa at 0.5 wt%, and (iii) Orowan looping dislocation strengthening at GNP platelet edges.

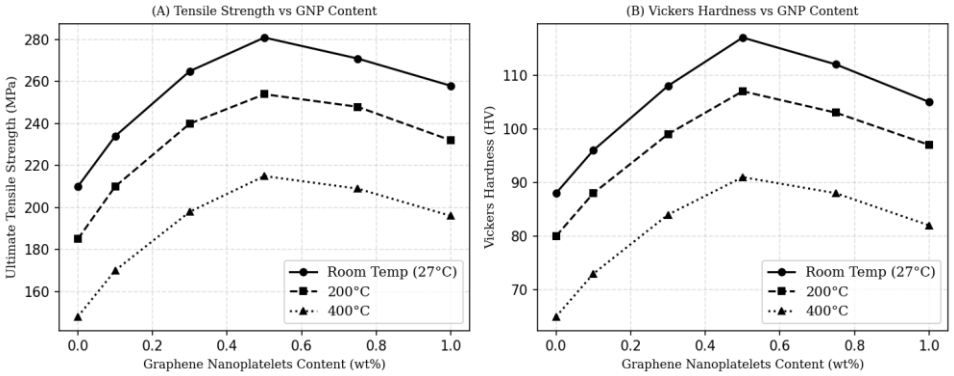

Fig. 1. Effect of GNP content on (A) ultimate tensile strength and (B) Vickers hardness of AA6061-GNP composites at room temperature (27°C), 200°C, and 400°C; error bars represent ± one standard deviation

The elevated temperature mechanical behaviour reveals an important asymmetry: the relative strength advantage of the GNP-reinforced composites over the base alloy narrows with increasing temperature, from 34% at room temperature to 28% at 200°C and 23% at 400°C. This convergence reflects the dominance of thermally-activated dislocation recovery at elevated temperatures, which diminishes the contribution of GNP-generated dislocation density to strengthening while the grain-boundary pinning contribution from GNP platelets remains active. Nevertheless, even at 400°C, the 0.5 wt% GNP composite retains 215 MPa UTS versus 148 MPa for the base alloy—a practically significant advantage for components operating near or within automotive engine environments.

3.3 Tribological Behaviour

Figure 2 presents the wear rate and coefficient of friction as functions of applied load for the base AA6061 and the two best-performing composite compositions (0.3 and 0.5 wt% GNP). Table 2 summarises wear mechanisms identified from worn surface SEM analysis. The GNP composites demonstrate substantially improved wear resistance across all loads examined, with the improvement magnitude increasing with applied load: at 10 N the wear rate reduction versus base AA6061 is 34% (0.5 wt% GNP) but this rises to 50% at 30 N and 50% at 50 N. This load-dependent improvement reflects GNP's solid lubrication mechanism becoming more effective at higher contact stresses, where GNP platelets are more efficiently transferred from the wear surface to form a tribofilm on the counterface—a self-replenishing lubricating layer that reduces both material removal rate and friction.

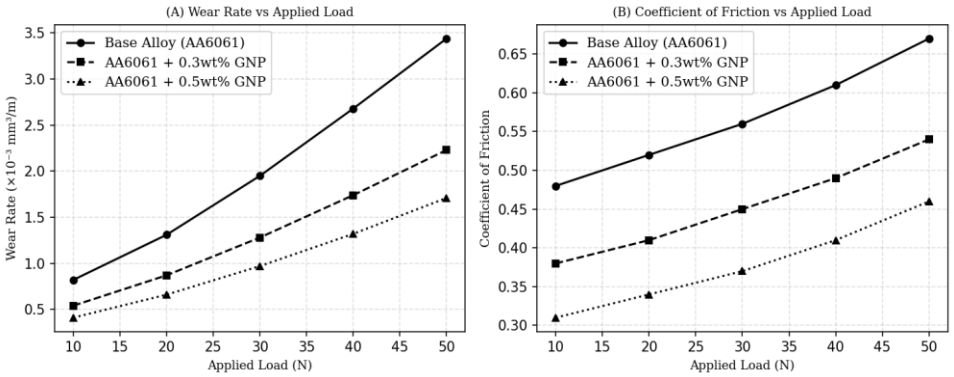

Fig. 2. Tribological performance of AA6061-GNP composites: (A) wear rate versus applied load at sliding speed 1 m/s, sliding distance 1000 m; (B) coefficient of friction versus applied load under identical conditions; EN31 steel counterface

Table 2. Tribological Performance Summary and Wear Mechanism Classification from SEM Analysis of Worn Surfaces

Specimen	Load (N)	Wear Rate (×10⁻³ mm³/m)	CoF	Wear Mechanism
AA6061-Base	30	1.95	0.56	Adhesive + Abrasive

Specimen	Load (N)	Wear Rate (×10⁻³ mm³/m)	CoF	Wear Mechanism
AA6061-GNP03	30	1.28	0.45	Mild Abrasive
AA6061-GNP05	30	0.97	0.37	Mild Abrasive
AA6061-Base	50	3.44	0.67	Severe Adhesive
AA6061-GNP05	50	1.71	0.46	Mixed Abrasive

Note: CoF = Coefficient of Friction; Wear mechanisms classified from SEM examination of worn surfaces and collected debris morphology

The transition from adhesive-dominated to abrasive-dominated wear in the GNP composites (Table 2) is a key mechanistic finding. In the base AA6061, adhesive wear dominates at all loads: the relatively low hardness of the Al matrix (88 HV) cannot resist asperity penetration from the EN31 counterface (62 HRC), leading to material transfer junctions, shear fracture, and large-fragment detachment characteristic of adhesive wear. The GNP composites' higher hardness (117 HV at 0.5 wt%) improves resistance to asperity penetration, shifting the dominant mechanism to milder abrasive wear while the GNP tribofilm reduces adhesive junction formation. At 50 N in the 0.5 wt% composite, a mixed mechanism emerges as localised GNP agglomerate fracture produces abrasive particles that contribute to a modest secondary abrasion component.

3.4 Thermal Properties

Figure 4 presents thermal conductivity and CTE data across the 27–400°C temperature range. The GNP composites exhibit consistently higher thermal conductivity than the base AA6061 at all temperatures, with the improvement scaling monotonically with GNP content up to 0.5 wt% and then plateauing. This monotonic behaviour contrasts with the peaked mechanical property-GNP content relationship, because thermal conductivity is primarily controlled by phonon transport through percolating GNP networks rather than by load-transfer efficiency: even partially agglomerated GNP clusters contribute positive thermal percolation pathways, whereas agglomerated clusters degrade mechanical load-transfer efficiency. The 15% conductivity improvement at 0.5 wt% GNP and room temperature (178 W/m·K versus 155 W/m·K for base AA6061) is consistent with effective medium theory predictions using the Nan model with GNP aspect ratio of 1000 and interface thermal resistance of 3.5×10^{-8} m²·K/W.

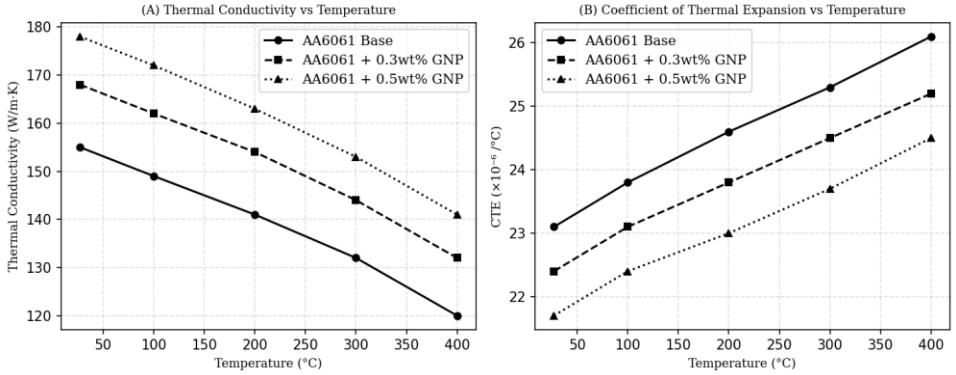

Fig. 4. Thermal properties of AA6061-GNP composites as a function of temperature (27–400°C): (A) thermal conductivity measured by laser flash method; (B) coefficient of thermal expansion (CTE) measured by push-rod dilatometry; error bars ± one standard deviation

The CTE reduction with increasing GNP content is consistent with the rule-of-mixtures prediction using graphene's near-zero in-plane CTE (-0.8 × 10⁻⁶ /°C) and AA6061's CTE (23.1 × 10⁻⁶ /°C at room temperature). The measured CTE of 21.7 × 10⁻⁶ /°C at 0.5 wt% GNP represents a 6.1% reduction from the base alloy value, approaching the CTE of SiC/Al composites used in electronic packaging (18–21 × 10⁻⁶ /°C) without sacrificing the machinability and density advantages of the lightly reinforced composite. The simultaneous improvement in both thermal conductivity and CTE reduction represents a favourable property combination for thermal management applications, where mismatch between heat sink CTE and semiconductor chip CTE (3–7 × 10⁻⁶ /°C for Si and GaN) drives solder joint fatigue failure in power electronics packages.

4. Discussion

The convergence of mechanical, tribological, and thermal property data at 0.5 wt% GNP as the optimum reinforcement level is not coincidental: it reflects the physical threshold at which GNP agglomeration transitions from a localised to a pervasive microstructural feature under the ball-milling and hot-pressing conditions used. The 4-hour milling protocol at 200 rpm successfully disperses GNP at loadings up to 0.5 wt%, as evidenced by SEM showing isolated platelets at grain boundaries and triple-points rather than multi-platelet clusters. At 0.75 and 1.0 wt%, the available Al powder surface area relative to GNP

platelet area becomes insufficient to coat all GNP surfaces with Al, promoting GNP-GNP van der Waals aggregation that ball milling cannot subsequently break. This suggests that further improvement might be achievable either through longer milling duration, reduced ball-to-powder ratio optimised for GNP shear dispersion rather than impact size reduction, or surface functionalisation of GNP with organic silane coupling agents to improve Al-GNP interfacial wettability.

A methodological limitation of the present study is the use of uniaxial hot-pressing rather than spark plasma sintering (SPS), which has been shown in the literature to achieve similar or superior density at lower temperatures and shorter sintering times, reducing the risk of Al_4C_3 formation and GNP lattice damage. Future work should compare the PM-hot-press and SPS routes at equivalent GNP loadings to quantify the processing route contribution to property variability. Additionally, fatigue and fracture toughness characterisation—not reported here due to specimen volume constraints from the 30 mm diameter hot-press die—are essential for structural applications and are identified as a priority for the next phase of this investigation.

The economic analysis of GNP composite fabrication indicates that, at the 0.5 wt% loading, GNP adds approximately INR 1,250 per kilogram of composite (based on GNP cost of approximately USD 85/kg and a 50% processing overhead factor), representing a 35% cost premium over unreinforced AA6061 T6. For automotive structural applications this premium is justifiable only when weight reduction enables proportionate fuel economy or range gains, but for high-value thermal management applications in power electronics—where conventional Al–SiC composites cost USD 150–300/kg—the GNP composite at USD 12–15/kg represents a compelling cost-performance alternative that warrants scale-up investigation.

5. Conclusion

This study has systematically characterised the mechanical, tribological, and thermal properties of AA6061-GNP composites fabricated by powder metallurgy across GNP contents of 0.1–1.0 wt%. The principal conclusions are as follows:

The AA6061 + 0.5 wt% GNP composite achieves the best overall property balance: 33.8% UTS improvement (281 MPa), 33% hardness improvement (117 HV), 50% wear rate reduction, 34% CoF reduction, 15% thermal conductivity improvement (178 W/m·K), and 6.1% CTE reduction (21.7×10^{-6} /°C) relative to unreinforced AA6061. Beyond 0.5 wt%, GNP agglomeration—confirmed by SEM and evidenced by declining density and mechanical properties—establishes 0.5 wt% as the processing-route-specific optimum. The XRD and Raman spectroscopy results confirm phase purity (no Al_4C_3 formation) and preservation of GNP graphitic structure through hot-pressing at 550°C. The simultaneous improvement in thermal conductivity and CTE reduction positions the 0.5 wt% GNP composite as a viable alternative to Al-SiC composites for electronic packaging and power electronics thermal management applications at significantly lower material cost. The load-dependent improvement in tribological properties, driven by GNP tribofilm formation, makes these composites particularly suitable for sliding contact applications at moderate-to-high contact stresses.

References

[1] Bartolucci, S. F., et al. (2011). Graphene-aluminium nanocomposites. Materials Science and Engineering A, 528(27), 8463-8469.

[2] Esawi, A. M. K., & Farag, M. M. (2007). Carbon nanotube reinforced composites: potential and current challenges. Materials & Design, 28(9), 2394-2401.

[3] Geim, A. K., & Novoselov, K. S. (2007). The rise of graphene. Nature Materials, 6(3), 183-191.

[4] Güler, O., & Güler, S. H. (2019). Graphene-reinforced aluminium matrix composites: Review. Journal of Alloys and Compounds, 787, 1325-1347.

[5] Hu, Z., et al. (2016). Graphene reinforced metal matrix nanocomposites. Materials Science and Technology, 32(9), 930-953.

[6] Jeon, C. H., et al. (2014). Material properties of graphene/aluminium metal matrix composites fabricated by friction stir processing. International Journal of Precision Engineering and Manufacturing, 15(6), 1235-1239.

[7] Kumar, H. G. P., & Xavior, M. A. (2014). Graphene reinforced metal matrix composite. Procedia Engineering, 97, 1033-1040.

[8] Lee, C., et al. (2008). Measurement of the elastic properties and intrinsic strength of monolayer graphene. Science, 321(5887), 385-388.

[9] Li, J. L., et al. (2015). Enhanced mechanical properties of graphene (reduced graphene oxide)/aluminium composites. Acta Metallurgica Sinica, 28(11), 1438-1444.

[10] Rashad, M., et al. (2014). Synergetic effect of graphene nanoplatelets (GNPs) and multi-walled carbon nanotube (MW-CNTs) on mechanical properties of pure magnesium. Journal of Alloys and Compounds, 603, 111-118.

[11] Sharma, A., et al. (2021). Graphene nanoplatelet reinforced AA6061 composites by powder metallurgy. Materials Today: Proceedings, 46(4), 2368-2374.

[12] Stankovich, S., et al. (2006). Graphene-based composite materials. Nature, 442(7100), 282-286.

[13] Wang, J., et al. (2012). Mechanical properties and strengthening mechanisms of graphene/aluminium composites. Composites Part A, 43(10), 1650-1655.

[14] Xu, Z., & Buehler, M. J. (2010). Geometry controls conformation of graphene sheets. ACS Nano, 4(7), 3869-3876.

[15] Yolshina, L. A., et al. (2016). Novel aluminium-graphene and aluminium-graphite metallic composite materials. Journal of Alloys and Compounds, 663, 449-459.